



ELSEVIER

Nuclear Instruments and Methods in Physics Research A 477 (2002) 256–261

**NUCLEAR  
INSTRUMENTS  
& METHODS  
IN PHYSICS  
RESEARCH**  
Section A

www.elsevier.com/locate/nima

# Position sensitive anodes for MCP read-out using induced charge measurement

O. Jagutzki<sup>a,\*</sup>, J.S. Lapington<sup>b</sup>, L.B.C. Worth<sup>b</sup>, U. Spillman<sup>a</sup>, V. Mergel<sup>a</sup>,  
H. Schmidt-Böcking<sup>a</sup>

<sup>a</sup>*Institut für Kernphysik, University Frankfurt, August Euler Strasse 6, 60486 Frankfurt, Germany*

<sup>b</sup>*Mullard Space Science Laboratory, Department of Space and Climate Physics, University College London, UK*

---

## Abstract

We investigate the method of an indirect detection of a MCP charge avalanche projected onto a resistive layer (G. Battistoni, et al., Nucl. Instr. and Meth., 202 (1982) 459). If the sheet resistance is favourable one can detect the charge cloud by the capacitive coupling to an anode structure a few millimetres behind the layer. The anode structure can be, for example, a wedge-and-strip electrode pattern (M. Unverzagt, Diplomarbeit, Universität Frankfurt 1992, private communication) as it is used for directly collecting the electron avalanche from a MCP.

Detection of the induced charge is beneficial in several respects. Firstly, image distortions produced by secondary electron mediated charge redistribution are eliminated. Secondly, the noise component due to quantized charge collection, commonly referred to as partition noise, is not present. In addition, the dielectric substrate can function both as an element of the vacuum enclosure and HV insulator, making the electrical connections easily accessible and the pattern operable at ground potential, independently of detector operating voltages. This technique can be used to simplify the electronic design requirements where varying high voltages are required at the detector input face such as plasma analysers, etc. It also has application in the manufacture of intensifier tubes (J. Barnstedt, M. Grewing, Nucl. Instr. and Meth., these proceedings) where the inclusion of a readout pattern inside the intensifier body with associated electrical feed-throughs can prove problematic.

We will present data on the performance of such detection geometries using several types of charge division anode, and discuss the advantages compared with the “traditional” charge collecting method. © 2002 Elsevier Science B.V. All rights reserved.

*Keywords:* Microchannel-plate; Imaging; Delay-line; Wedge-and-strip; Induced charge

---

## 1. Wedge-and-strip anode with the image charge method

The manufacture and operation of an image charge wedge-and-strip anode (WSA) has proven to be very straightforward. For this experiment, we used an existing WSA pattern, manufactured with our laser machining process, and using

---

\*Corresponding author. Tel.: +49-69-79824276; fax: +49-69-79824212.

E-mail address: jagutzki@hsb.uni-frankfurt.de (O. Jagutzki).

copper conductors on a 2 mm thick fused silica substrate. The WSA pattern had a pitch of 1 mm and active area of 40 mm diameter. The resistive layer [1] was manufactured by sputter coating with germanium. Initially, we used RF sputtering and this produced ideal resistivity for the first device. We have since experimented with DC sputtering but the high deposition rate is difficult to attenuate sufficiently to achieve a suitable resistivity.

The detector utilized a chevron stack of Photonic MCPs, each with a length to diameter ratio of 120:1. The configuration allowed us to use the same WSA for electron collection, and induced charge imaging, allowing us to compare performance directly. Fig. 1 shows two images of pinhole masks at count rates of 400 and 151 kHz, respectively, taken with the detector in the image charge configuration. The pinhole masks were  $19\ \mu\text{m}$  diameter  $\times$  0.5 mm pitch, and  $35\ \mu\text{m}$  diameter  $\times$  0.8 mm pitch, respectively. The MCPs had undergone rigorous use, and the resulting areas of gain depression can clearly be seen at high count rates in Fig. 1b.

This and other data were used to compare WSA performance between collected and induced charge collection [2,3]. Fig. 2a is a plot of the resolution versus input count rate showing data taken in both modes. At higher count rates, the resolution degrades mainly due to the combination of pulse pile-up in the electronics, and gain depression [4] from the localized high count rate in the microchannel plate. Even so, the resolution versus count rate graph shows that spatial accuracy is little more than  $100\ \mu\text{m}$  FWHM even at 150 k counts per second. Results using electron collection at lower rates are shown for comparison. No pile-up rejection was used and only a small fraction of events were collected owing to limitations at the computer interface.

Image resolution is very similar in both modes; the loss of induced signal in the image charge mode being compensated for by the absence of both partition noise and possible centroiding errors caused by inhomogeneity in the charge cloud. The positions of the central pinhole images from Fig. 1a are plotted in Fig. 2b. We were unable to proximity focus the anode in the image charge mode owing to the in-built geometry

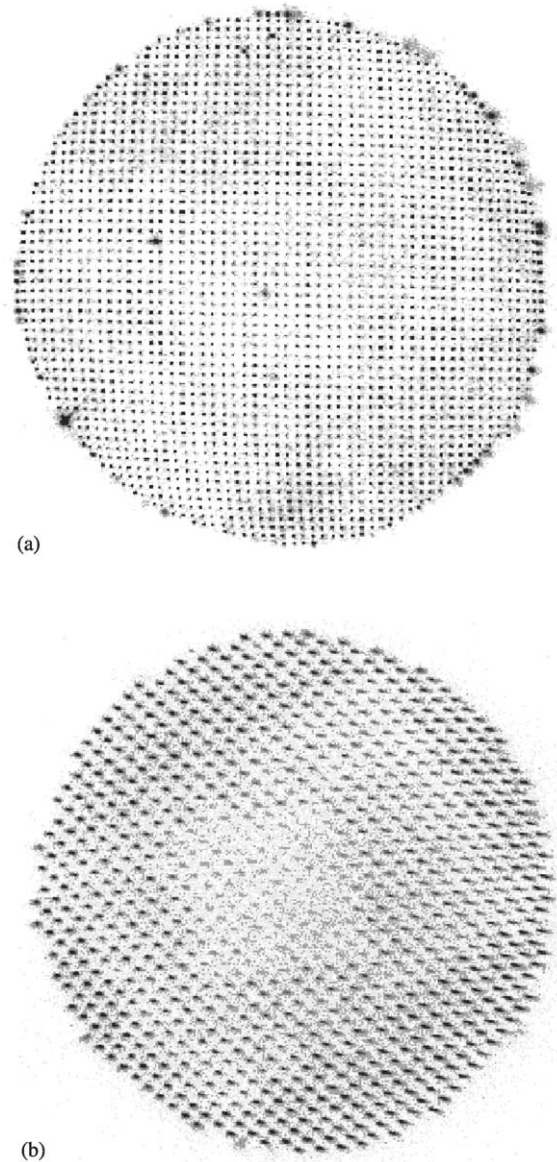


Fig. 1. Images taken with a WSA at low and high count rates. (a) Shows the image of a 0.5 mm pitch pinhole mask. The image resolution is less than  $40\ \mu\text{m}$  FWHM. This degrades to  $\sim 100\ \mu\text{m}$  at 150 kHz as shown in (b). The rectangular shadow is caused by gain fatigue in areas of the microchannel plate which have suffered prolonged illumination.

required for electron collection. Electrostatic effects near the active perimeter are the dominant cause of the distortions, despite a high drift field. These will be diminished by proximity focusing. At

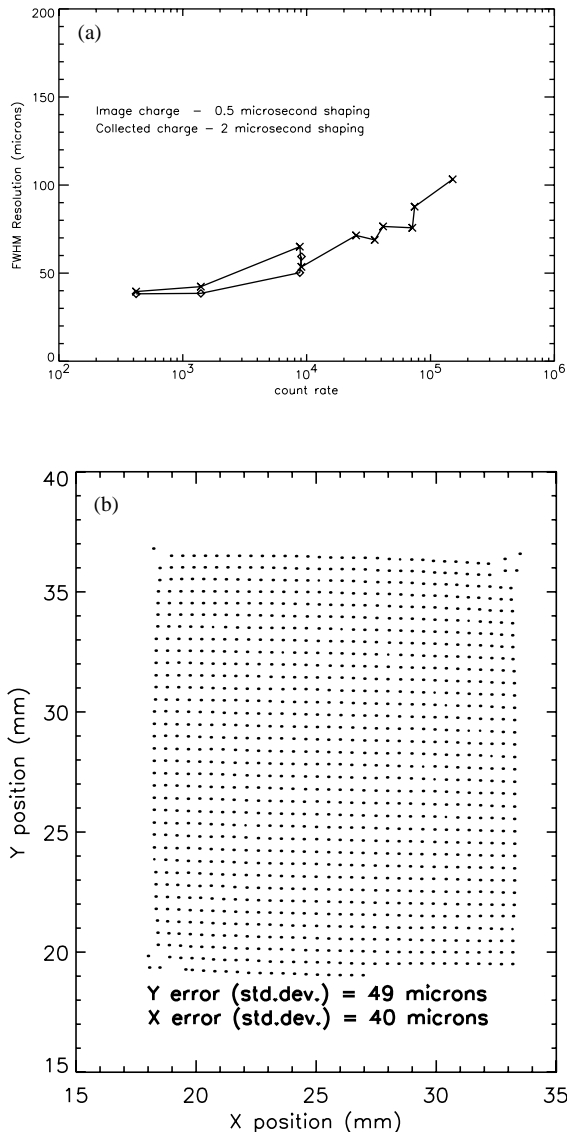


Fig. 2. (a) Is a plot of the image resolution of a WSA versus count rate for electron collection and image charge modes. (b) Shows the linearity of the central region of Fig. 1a. The nonlinearity in this region is 40–50  $\mu\text{m}$  rms.

present, the electrostatic distortion caused by the lower MCP contact intrudes into the imaging area owing to the unnecessary 6 mm drift region between MCP and anode. The measured linearity of the central region, shown in Fig. 2b, is 40 and 49  $\mu\text{m}$  standard deviation in  $x$  and  $y$ ,

respectively. Over the whole image 81 and 70  $\mu\text{m}$ , respectively.

We intended to demonstrate the image charge Vernier anode [5] performance for this paper, but encountered the increased Germanium DC sputtering deposition rate, discussed earlier, during its manufacture. The lower resistivity produced a larger induced charge footprint, for a given electronic shaping time, which compromised the Vernier performance. However, imaging was still achieved albeit with a lower resolution. We expect the image charge technique to improve the Vernier anode's current resolution of 10  $\mu\text{m}$  FWHM due to the removal of partition noise and charge centroid, and to further improve linearity by eliminating secondary electron effects on the anode.

## 2. Delay-line read-out with the image charge method

Charge integration techniques applied for single particle imaging generally suffer from the fact that rather slow analogue electronic circuits need to be applied. That principally limits the rate acceptance of the detector. A method that maintains good position resolution even at high rates is the delay-line technique [6]. Here, only fast timing electronic circuits are used and modern digitisation concepts even presume this read-out speed for the data acquisition.

In comparison to the W&S-type read-out, it is not as straightforward to operate a common delay-line anode, designed for electron cloud collection, in image charge mode. For example, the helical wire anode [7] definitely needs to collect “real” electrons to function properly. Other anode types will likely suffer from cross talk between electrode structures as the electromagnetic image charge cannot be steered with electrostatic potentials or partially shielded, as is possible with real charges. We discovered that the crossed strip anode [8], though having outstanding imaging performance for real charge detection, does not give useful results via image charge detection. Presumably, the intermediate “ground” electrode layer also picked up the image charge and thus was not effective as a cross talk shield any more.

We have designed a delay-line anode that overcomes these problems [9]. The image charge pick-up electrode pattern is made up by diamonds connected in rows for each dimension, and leading to an external meander delay-line. Fig. 3 shows a photograph and the detail from the corner of the pattern. A similar design was previously applied by Eland [10]. The collecting “fingers” for

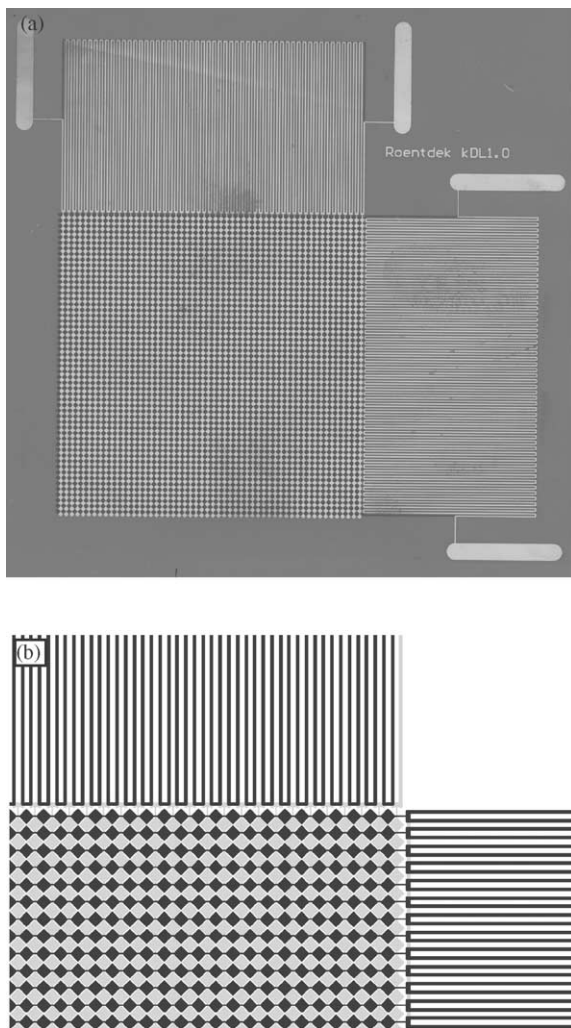


Fig. 3. The diamond-delay-line anode (front side) and corner detail showing the electrode design. The structures are produced by standard industrial line photo-etching on a  $40\mu\text{m}$  two-layer Kapton substrate with  $25\mu\text{m}$  copper. The pitch distance is  $1\text{mm}$ , the square collection area measures  $54\text{mm}$ .

each dimension are placed on different sides of a thin Kapton substrate. Thus the manufacturing is very easy and cross talk between  $x$  and  $y$  electrodes is sufficiently suppressed just by the geometry of the electrodes, having only very little area overlap. The delay lines are formed in shifted double meander line configuration, with one line connected to the respective fingers, the other “ground” line being placed on the opposite side of the sub-strate. The signals are picked up by differential amplifiers.

Fig. 4 shows the image resolution, and Fig. 5, the linearity performance of the diamond-delay-line anode. The transmission properties of this meander line were not yet optimized, leading to significant damping on the line. However, we could already achieve a rather uniform detector response. The anode was placed in contact with the rear side of an  $\text{Al}_2\text{O}_3$ -ceramic wafer of  $1.2\text{mm}$  thickness; the front side coated with  $100\text{nm}$  Ge. A  $40\text{mm}$  active MCP stack (chevron of Photonis 1:80,  $12.5\mu\text{m}$  pore) operated at  $2850\text{V}$  gave sufficient charge output to compensate for the signal damping problem on the transmission line. However, we expect the imaging performance to improve further with proper transmission line design.

Little is known about the time dependence, on the nanosecond scale, of the charge cloud footprint on the resistive sheet so far. From earlier tests with one-dimensional delay-line anodes of similar design [11] it was found that the resistive layer can impose a certain rate limitation. With a  $100\text{nm}$  Ge layer as resistive sheet, the transmitted signal height was reduced when the count rate ( $2\text{keV}$  Ar ions) exceeded  $1\text{MHz}$ . This could be improved by increasing the Ge layer thickness, i.e. the reduced sheet resistance restoring the performance.

Using the 2d detector, we have not been able to maintain the currently required very high MCP gain for UV-photon fluxes beyond  $300\text{kHz}$ . However, we could verify that even at such rate no apparent image degradation takes place.

### 3. Summary and outlook

The image charge technique has major benefits for detector and readout design alike.

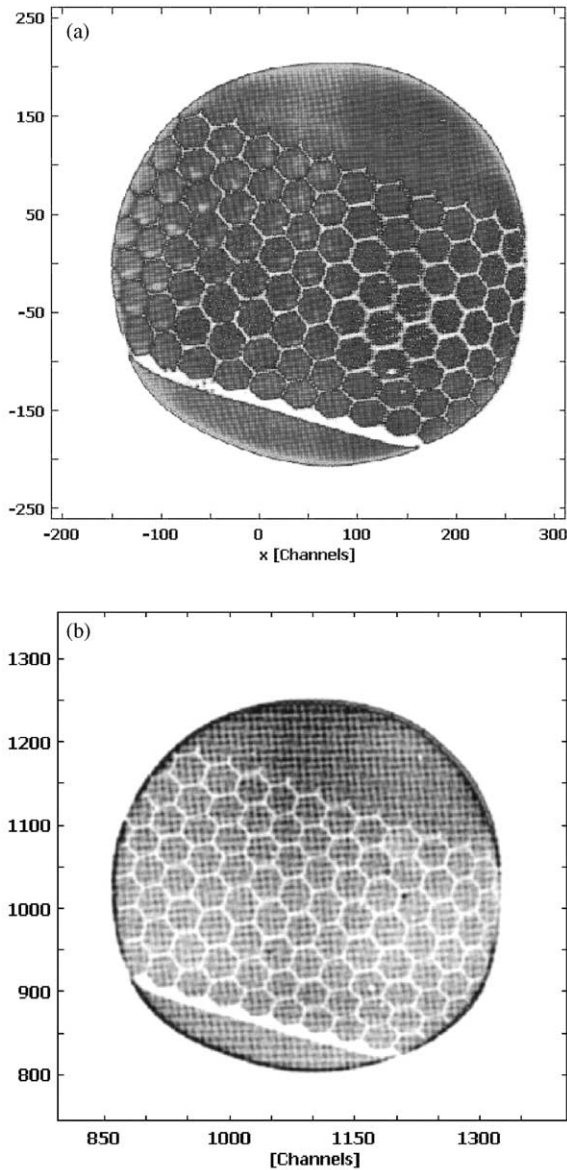


Fig. 4. The image resolution of the diamond-delay-line anode. The detector was shaded by a hexagonal mask (3 mm hexagons, 0.2 mm obstacle) and underlying by a grid mask of  $600\ \mu\text{m}$  grid constant and  $70\ \mu\text{m}$  obstacle. (a) Shows the detector homogeneously illuminated with  $\alpha$ -particles at a low rate. (b) Is the same as above, but illuminated with UV-photons at 350 kHz. The TDC used limits the position resolution to about  $80\ \mu\text{m}$ .

(i) The readout can be proximity focused to the anode and a well defined charge footprint can be induced on the readout through the

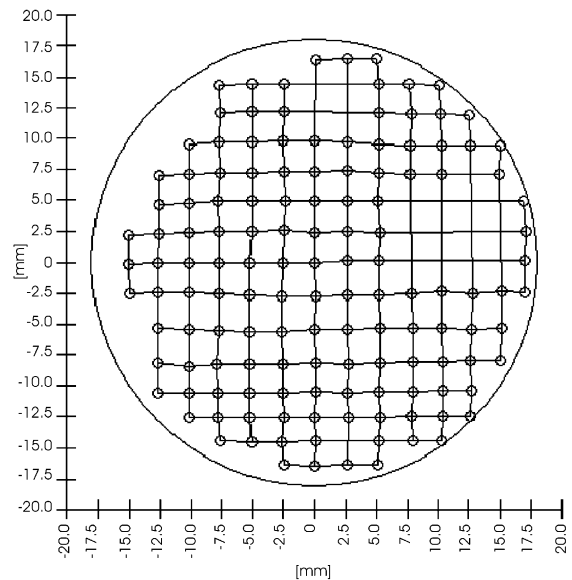


Fig. 5. The linearity performance of the diamond-delay-line anode. The mean deviation from linearity is 120 and  $410\ \mu\text{m}$  in the x- and y-axis respectively.

substrate without resorting to an MCP to anode drift region. This makes the detector less liable to electrostatic distortions and magnification of charge centroid errors, which can occur with a drift region.

- (ii) The readout is electrically isolated from the detector. The germanium resistive layer can be operated at high voltage while the readout is at ground potential, simplifying electronic design, giving greater ease of operation, and increasing the immunity from HV noise and breakdown.
- (iii) An image intensifier design utilizing this technique can use an external pattern, avoiding processing of the readout during tube manufacture, and the need for multiple electrical feedthroughs.
- (iv) Charge division readouts benefit from image charge in several ways. Using induced charge, they do not suffer from partition noise, which results from the statistics of collection of quantized charge. Problems such as image instability and nonlinearity associated with secondary electron production on the anode,

and related effects such as charge redistribution, are avoided.

Future areas of development include investigation of the image charge devices at high count rates to determine the effect of the germanium sheet resistivity and find an optimum value. The design of the image charge two-dimensional delay line described above, will be modified to improve performance further. We intend to demonstrate the operation of the image charge technique with pixel-type readouts.

The benefits accrued by applying the image charge technique to image intensifiers will be exploited by developing a generic tube design, suitable for various readout types. We intend to demonstrate performance of delay-line, Vernier, and pixel readouts in this application.

## References

- [1] G. Battistoni, P. Campana, V. Chiarella, U. Denni, E. Iarocci, G. Nicoletti, Nucl. Instr. and Meth. 202 (1982) 459.
- [2] M. Unverzagt, Diplomarbeit, Universität Frankfurt 1992, private communication.
- [3] J. Barnstedt, M. Grewing, Nucl. Instr. and Meth. A 477 (2002) 268, these proceedings.
- [4] M.L. Edgar, J.S. Lapington, A. Smith, Rev. Sci. Instr. 63 (1992) 816.
- [5] J.S. Lapington, B. Sanderson, L.B.C. Worth, Nucl. Instr. and Meth. A 477 (2002) 250, these proceedings.
- [6] O. Jagutzki, V. Mergel, K. Ullmann-Pflegger, L. Spielberger, U. Spillmann, R. Dörner, H. Schmidt-Böcking, Nucl. Instr. and Meth. A 477 (2002) 244, these proceedings.
- [7] S.E. Sobottka, M.B. Williams, IEEE Trans. Nucl. Sci. 35 (1988) 348.
- [8] O.H.W. Siegmund, et al., Proc. SPIE 2280 (1994) 89.
- [9] O. Jagutzki, J. Barnstedt, U. Spillmann, L. Spielberger, V. Mergel, K. Ullmann-Pflegger, M. Grewing, H. Schmidt-Böcking, Proc. SPIE 3764, in press.
- [10] J.H.D. Eland, Meas. Sci. Technol. 5 (1994) 1501.
- [11] U. Meyer, Diplomarbeit, Universität Frankfurt 1995, private communication.